

Biodegradable Electrohydraulic Soft Actuators

Ryo Kanno, Fabio Caruso, Kazuma Takai, Yegor Piskarev, Vito Cacucciolo, and Jun Shintake*

Biodegradable materials decompose and return to nature. This functionality can be applied to derive robotic systems that are environmentally friendly. This study presents a fully biodegradable soft actuator, which is one of the key elements in “green” soft robotics. The working of the actuator is based on an electrohydraulic principle, which is similar to that of hydraulically amplified self-healing electrostatic actuators. The actuator developed in this study consists of a dielectric film made of polylactic acid (PLA) and polybutylene adipate-co-terephthalate (PBAT), with soybean oil as the dielectric liquid and electrodes made from a mixture of gelatin, glycerol, and sodium chloride (NaCl). The synthesized biodegradable electrode material exhibits a Young’s modulus of 0.06 MPa and resistivity of 258 $\Omega\cdot\text{m}$ when the mass fraction of NaCl relative to the amount of gelatin and glycerol is 10 wt%. The softness and resistivity of the electrode material results in actuation strain values of 3.2% (at 1 kV, corresponding to 1.2 kV mm^{-1}) and 18.6% (at 10 kV, corresponding to 9.6 kV mm^{-1}) for the linear-type and circular-type actuators, respectively. These values obtained for the biodegradable electrohydraulic soft actuators are comparable to those of nonbiodegradable actuators of the same type, representing the successful implementation of the concept.

1. Introduction

Soft robotics has a high potential owing to the high compliance from which a wide variety of functional robots and applications can be derived.^[1–8] Synthetic polymers such as silicone rubbers and acrylic polymers are the most widespread materials used in soft robotics. They are low cost,^[9] easy to handle,^[10] and compatible with various fabrication methods, such as casting, molding,^[11] printing,^[12] and cutting.^[13] Silicone rubbers and acrylic polymers are also chemically stable, making them suitable for soft robots operated in diverse situations and environments, such as on the ground,^[14,15] underwater,^[16,17] in snowstorms,^[18] and even in radiation environments.^[19] On the contrary, their stable nature and irreversible synthetic process, like thermoset,^[20,21] make them nonbiodegradable, which may lead to environmental destruction; this can particularly occur when the robots performing tasks in natural fields are discarded due to malfunctions

or accidents. As an example of environmental impact, it has been reported that some fishes have silicone rubbers and acrylic polymers that are not degraded and deposited in their bodies.^[22,23] In addition, polymeric materials used in soft robotics are mostly difficult to recycle and have a high environmental impact. Considering these perspectives, it is important to incorporate biodegradability into soft robots.

Researchers have demonstrated biodegradable soft robotic elements that are focused on actuators. Their working principle includes pneumatic actuation,^[24–30] piezoelectricity,^[31] ion migration,^[32–36] and swelling.^[37,38] Pneumatic actuators are relatively easy to fabricate and can provide large outputs; however, their performance is dependent on bulky external pumps and compressors, which can lead to difficulty in constructing robots according to their types and specifications. From a system perspective, actuators based on piezoelectricity and ion migration have been driven electrically using a portable power source. However, actuation strain generated by piezoelectricity tends to be small (4%^[39]) and the actuation speed achieved with ion migration is normally low (2.3% s^{-1} ^[40]), thus limiting the actuation performance. Similarly, actuation based on swelling has a limitation on speed (over 6 h required for achieving a fully swelled state^[37]) and controllability of actuated deformation because its working principle requires material injection^[37] and cannot perform multiple actuations.^[38]

R. Kanno, K. Takai, J. Shintake
Department of Mechanical and Intelligent Systems Engineering
The University of Electro-communications
1-5-1 Chofugaoka, Chofu, Tokyo 182-8585, Japan
E-mail: shintake@uec.ac.jp

F. Caruso, V. Cacucciolo
Department of Mechanics, Mathematics and Management
Politecnico di Bari
via E. Orabona n. 4, 70125 Bari, Italy

Y. Piskarev
Laboratory of Intelligent Systems
Institute of Mechanical Engineering
School of Engineering
École Polytechnique Fédérale de Lausanne
1015 Lausanne, Switzerland

 The ORCID identification number(s) for the author(s) of this article can be found under <https://doi.org/10.1002/aisy.202200239>.

© 2023 The Authors. Advanced Intelligent Systems published by Wiley-VCH GmbH. This is an open access article under the terms of the Creative Commons Attribution License, which permits use, distribution and reproduction in any medium, provided the original work is properly cited.

DOI: 10.1002/aisy.202200239

In recent years, electrohydraulic soft actuators, also known as hydraulically amplified self-healing electrostatic (HASEL) actuators, are emerging.^[41] This type of actuators consists of a pair of opposing electrodes covering a portion of the surface of a flexible pouch encapsulating a dielectric liquid. When a high voltage is applied, electrostatic forces between the electrodes squeeze the pouch, causing the local position of the liquid to change, resulting in a hydraulic deformation of the entire structure as actuation. Electrohydraulic soft actuators exhibit large actuation strain (107% linear strain^[42]), high actuation stress (≈ 114 kPa^[42]) and power density (358 W kg⁻¹^[42]), and fast speed (strain rate of 900% s⁻¹^[43]). Their structure is simple, allowing their tailoring in various shapes.

In this article, we present a biodegradable soft actuator based on the electrohydraulic principle. This type of actuation principle requires compliant and conductive electrodes. First, we investigated the mechanical and electrical properties of the electrode for different compositions. Then, we fabricated and characterized two types of actuators that have linear and circular shapes to study the effect of incorporating biodegradable materials into the existing actuation principle and to validate our hypothesis. It is worth mentioning that Rumley et al. recently reported a

similar actuator concept.^[44] However, at the time we submitted our article and published it as a preprint,^[45] their article had not been published or submitted. Therefore, there was no possibility for us to have any knowledge of their work in the conduct of this study.

2. Results and Discussion

The linear and circular biodegradable electrohydraulic soft actuators developed in this study are shown in **Figure 1a,b** (see also Video S1, Supporting Information). Both actuators have a sandwich structure composed of two layers of dielectric film made of polylactic acid (PLA) and polybutylene adipate-co-terephthalate (PBAT), forming a pouch encapsulating soybean oil as the dielectric liquid. PLA/PBAT film is known as a biodegradable substrate with good processability.^[46] The pouch is made by welding two layers of dielectric film using a 3D printer. In the fabrication process, the dielectric films are first placed between two sheets of polyimide film. Then, the heated nozzle of the 3D printer traces over the polyimide film, including the dielectric films (see the Experimental Section for details of the fabrication process).

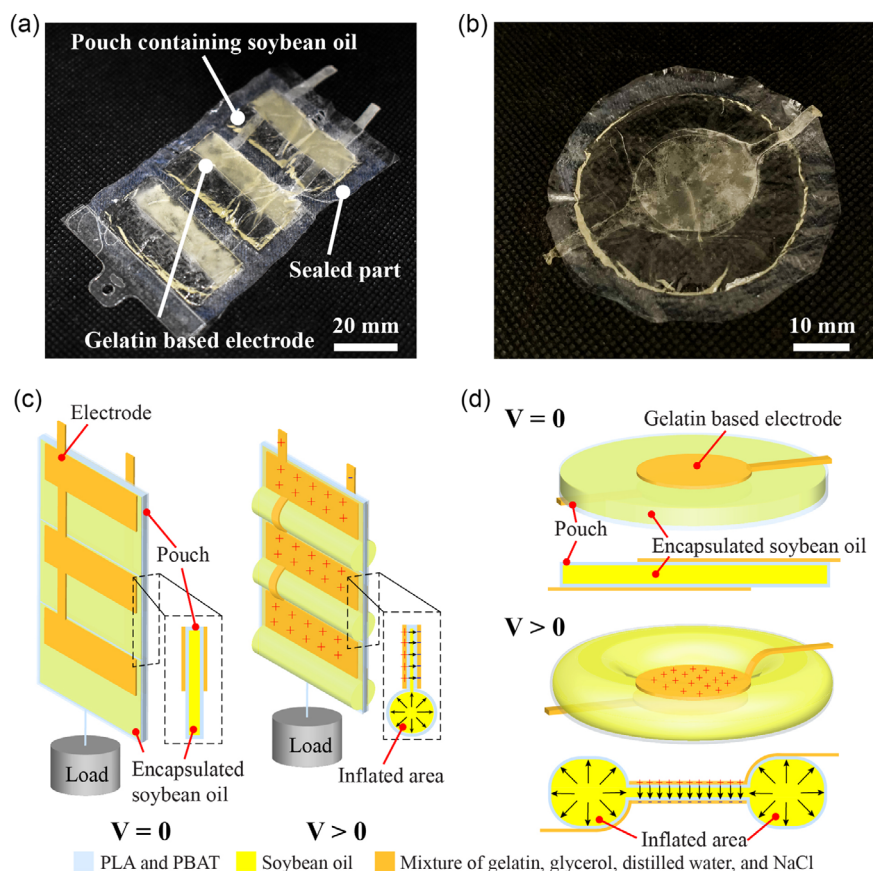


Figure 1. Biodegradable electrohydraulic soft actuators fabricated in this study. a) Linear-type actuator. The actuator has three pouches and sealed part for encapsulation of soybean oil. Gelatin-based electrodes are placed on both side of the actuator. b) Circular-type actuator consisting one pouch and sealed part. Gelatin-based electrodes are placed on both side of the actuator. c,d) Working principle of the linear-type actuator and the circular-type actuator. When voltage is applied, electrodes are charged, resulting in an electrostatic pressure that squeezes the pouch containing the soybean oil, which is placed in the areas where the electrodes do not overlap. The oil transferred in the nonelectrode areas inflates the pouch, causing deformation of the entire structure.

On the pouch, electrodes are attached, which consist of a mixture of gelatin, glycerol, and sodium chloride (NaCl) by intrinsic adhesion. The electrode material has an adhesive nature because of which it can be attached to the pouch without the need for glue. The entire surface of the device is covered by corn starch powder to keep the surface nonsticky. The integration of these materials and ingredients makes the actuator fully biodegradable. The geometry of our actuators is similar to those of the Peano-HASEL actuator and circle planar HASEL actuator available in the literature.^[42,43] Since the dielectric liquid used is soybean oil, which provides no self-healing ability, we cease to use the abbreviation HASEL in the rest of the article to avoid any confusion on the functionality.

The working principle of the linear and circular-type actuators is identical and is shown in Figure 1c,d. When voltage is applied, electrodes are charged, resulting in an electrostatic pressure. This pressure squeezes the pouch containing the soybean oil, which is placed in the areas where the electrodes do not overlap. The oil transferred in the nonelectrode areas inflates the pouch, causing deformation of the entire structure. In the linear-type actuator, the actuated deformation occurs as contraction. In the circular-type actuator, it leads to expansion. In the linear-type actuator, the dimensions of the pouch and electrode area are 40 mm × 20 mm and 38 mm × 10 mm, respectively. In the circular-type actuator, the inner diameter of the pouch and the diameter of the electrode are 50 and 25 mm, respectively. **Figure 2** shows a biodegradation process of a circular-type actuator. The temperature in the degradation environment was set to be 60 °C using an oven, where degradation of both protein and PLA-based biodegradable materials takes place in the composting environment, with reference to previous studies.^[47,48] The composting environment, simulated by a temperature of 60 °C, was chosen to accelerate the biodegradation process, as it is the only way to biodegrade PLAs in a shorter amount of time than in a natural environment.^[49,50] The device gradually degrades in the soil with time. Regarding the characteristics change of the actuator under biodegradation, it was expected that in the electrode the water content decreases, the resistivity increases, and the material hardens, as revealed in our previous study on mixture of gelatin and glycerol.^[27] For the dielectric film (PLA/PBAT), the molecular weight decreases by the soil decomposition of the film, as described in the literature.^[51] It is considered that the film becomes thinner and the barrier properties decrease after a certain period of time, leading to the leakage of soybean oil from the sealed part. In our experiment, it is observed that oil leaked one

month later when the actuator is placed on soil, as shown in Figure 2. As a whole, the actuation strain and pressure will decrease due to the hardening of the gelatin-based electrodes as degradation progresses. Additionally, the response speed will also decrease due to the increased resistivity.

2.1. Electrical and Mechanical Properties of Electrodes

We first assessed the electrical and mechanical properties of the electrode material to identify a composition suitable for the actuators. As mentioned previously, gelatin and glycerol were used as the base material of the electrodes. After curing, the mixture of gelatin and glycerol exhibited elastomer-like characteristics, such as high stretchability (up to 209.6% of strain) and durability (multiple operations).^[24,27] The ratio of gelatin and glycerol used in the present study is identical to the mixture used in our previous work (gelatin:glycerol = 2:1).^[24,27] Its electrical resistivity is ≈3500 Ω m according to our preliminary experiments, which limits the actuation of the biodegradable electrohydraulic soft actuators. High resistivity constrains the amount of electrical current passing through the electrodes, lengthening time for accumulating electric charges on the electrodes to produce electrostatic actuation, which slows down movement of the actuators. Hence, we employed NaCl as an additive for the gelatin–glycerol mixture to lower the resistivity (i.e., enhance the conductivity) and investigated its influence on the electrical and mechanical properties. Specifically, we measured the resistivity and Young's modulus of the electrode material for different amounts of NaCl (see Experimental Section for the details of the fabrication process of the electrodes and the measurements). The amounts of NaCl were 0, 0.23, 0.45, 0.69, 0.92, 1.25, 2.5, 3.75, and 5 g, which correspond to the mass fractions relative to the amount of gelatin and glycerol of 0, 0.5, 1.0, 1.5, 2.0, 2.7, 5.3, 7.7, and 10 wt%, respectively. Note that the mass fraction presented here does not include the presence of distilled water (initial mass 120 g) used in the mixing process of the electrode material. After curing, the water mostly evaporated and had an equilibrium state.

As shown in **Figure 3a**, the resistivity decreases with increasing fraction of NaCl. This indicates that the resistivity of the electrode material can be controlled by adjusting the amount of additive. For 10 wt%, the resistivity is 258 Ω m, which is comparable to nonbiodegradable stretchable electrodes used in electrostatic soft actuators (specifically, dielectric elastomer actuators) that have resistivity of 90–2250 Ω m.^[52]



Figure 2. Biodegradation process of the circular-type actuator. Immediately after fabrication, the actuator is placed on the soil, and the whole setup is contained in an oven to keep the temperature (60 °C) constant to encourage microbial activity.

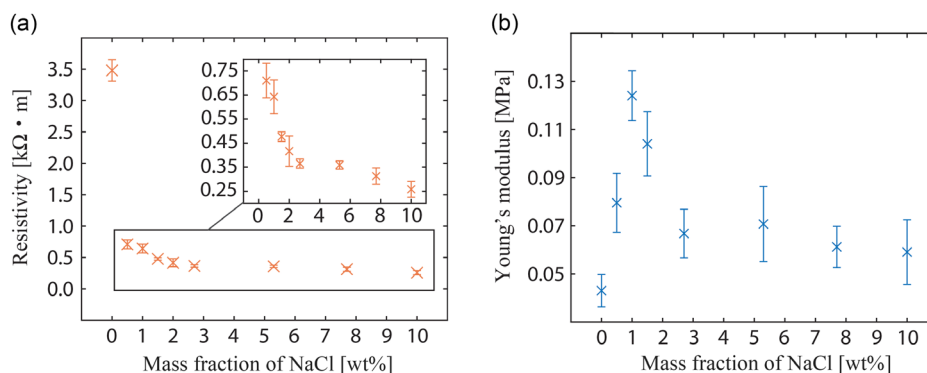


Figure 3. Characterization results of the gelatin-based electrodes. Changes in resistivity and Young's modulus were observed by changing the amount of sodium chloride added to the electrode. a) Resistivity as a function of the NaCl mass fraction. Average of four samples was used to determine the resistivity of each plot. b) Young's modulus as a function of the NaCl mass fraction. Four samples were averaged to determine the resistivity of each plot. The error bars represented in (a) and (b) are the standard deviations calculated from the four samples.

This suggests that our material is conductive and can provide electric actuation in the devices developed in this study. Figure 3b shows the plot of the measured Young's modulus of the electrode material. The modulus takes the lowest value of 0.04 MPa for 0 wt% and increases up to 0.12 MPa until 1.0 wt%. Interestingly, from 1.0 to 10 wt%, the modulus decreases from 0.12 MPa down to 0.06 MPa. The reason is as follows. Originally, gelatin binds to water molecules and forms a gel. Concurrently, sodium and chloride ions also bind to water molecules (binding force: enthalpy of hydration). This binding force is stronger in hydrated NaCl than in gelatin gel. Specifically, the binding force (van der Waals force) of gelatin molecules and water molecules is 0.4–4.0 kJ mol⁻¹.^[53] On the contrary, the enthalpies of hydration of sodium and chloride ions are over 300 kJ mol⁻¹.^[54] Therefore, hydrated NaCl binds the excess water in the sample (0–1.0 wt%) and hardens the electrodes, leading to a greater Young's modulus. However, from 1.0 to 10 wt%, the water molecules originally bonded to gelatin now bond to NaCl, resulting in a lower Young's modulus.

The results show a trade-off relationship between resistivity and compliance of the material. As shown in the range of 0–1.0 wt%, the resistivity decreases with increasing amount of NaCl, while the Young's modulus increases. Depending on the application, softer and more conductive electrodes are preferred, for instance, in soft electrically driven actuators. In this case, the presence of mechanically passive electrodes minimized the effect on actuation performance, and the electric current went through within a short time, thus ensuring a fast response. On the contrary, in some cases, it is difficult to pattern electrodes if they are too soft, making the fabrication complex.

2.2. Linear-Type Biodegradable Electrohydraulic Soft Actuators

We performed an electromechanical characterization of the linear-type biodegradable electrohydraulic soft actuator. In this test, strain as a function of the applied voltage was measured under different loading conditions (0, 5, and 20 g). Electrodes with a NaCl mass fraction of 10 wt% were used in the tested actuators. This is because they have a lower Young's modulus and the highest conductivity. The applied voltage was limited

to 1 kV, as it was found during a preliminary experiment that the actuators undergo electrical breakdown at voltages more than 1 kV. This is reasonable given the thickness (10 μm) and the dielectric strength of the film material (in the case of PLA, ≈33 kV mm⁻¹^[55] which corresponds to 660 V for two films). When actuated, the film layers of the pouch come closer owing to the electrostatic forces between the electrodes, resulting in the growth of the electric field strength. This zipping of the films starts from the top edge of the pouch where the electrodes are already closest even before applying the voltage, as represented in Figure S2, Supporting Information. In the zipped domain, most of the oil is transferred in the nonelectrode areas but we assume that meager amount of oil is existing like a layer between the films, resulting in the breakdown voltage of more than 1 kV.

Figure 4 shows the actuation and characterization results of the actuators. The relationships for other tested actuators with different amounts of NaCl in their electrodes are also shown in Figure S1, Supporting Information. As shown in Figure 4b, the actuation strain increases from 0% to 3.2%. Contrarily, the strain decreases under a larger applied load. The maximum strains in the tested voltage range for loading of 0, 5, and 20 g are 3.2%, 1.6%, and 0.5% respectively. The simulated values calculated by an analytical model (see Supporting Information for the details) exhibit the same trend as the experimental data, which suggests that the fabricated biodegradable actuators are functioning properly according to the fundamental working principle employed in this study. The main focus of our work is not modeling; nevertheless, the results indicate that it is possible to design biodegradable electrohydraulic soft actuators with the aid of models intended to be used for nondegradable actuators. However, there is a discrepancy between the simulation and the experiment on the strain at each voltage. This may result from the fact that the simulation assumes a 2D motion of the actuator, as shown in the cross-sectional view of Figure 1c. The actuator also moves in 3D motion, leading to actuation strains lower than the theoretical values. In addition, it also causes deformation of the sealed parts of the pouch (5-mm width) that is mechanically passive. Under actuated state, a portion of input electrical energy is stored in the sealed parts as mechanical bending energy, ultimately reducing the actuation strain.

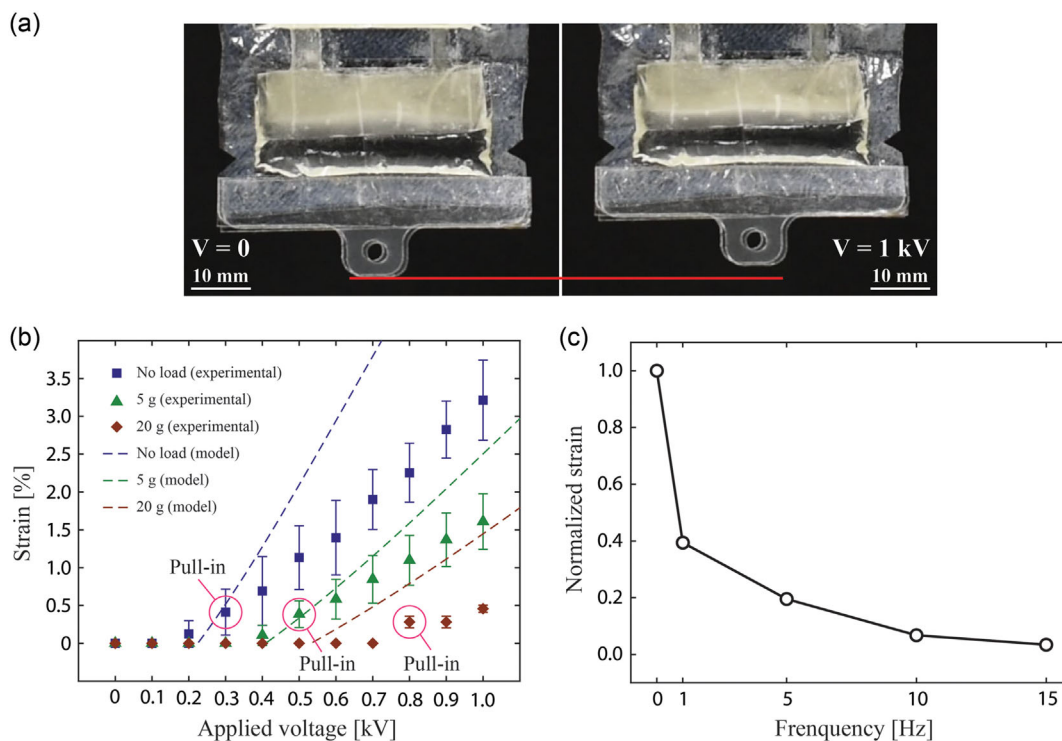


Figure 4. Characterization results of the linear-type actuators. a) Movement of the actuator. b) Actuation strain as a function of the applied voltage. The error bars represent the standard deviation calculated from the three samples. c) Actuation strain as a function of the applied voltage (5-g load, applied voltage 1 kV). The strain was normalized with reference to 0 Hz (DC).

At 1 kV, the measured strain of the biodegradable electrohydraulic soft actuators is 3.4%. This value is to that observed for nonbiodegradable actuators of the same type (the geometry and dimension of the pouch and the amount of dielectric fluid are identical); the Peano-HASEL exhibits an actuation strain of $\approx 5.4\%$ at 6 kV.^[43] This result indicates that biodegradable materials can be incorporated into electrically driven soft actuators without compromising the actuation strain. As we mentioned, the area of sealed parts negatively affects the actuation performance as it is a passive part. This also means that higher actuation strains may be achieved by reducing the area of the passive part.

We then assessed the frequency response of the actuator to estimate the specific power, which is a metric of output characteristics (see Supporting Information for the details). The result is represented as the normalized strain as a function of the driving frequency in Figure 4c. As can be seen from the plot, the strain gradually decreases as the frequency increases. The maximum specific power, calculated from Equation (13) in the Supporting Information and the data shown in Figure 5, is 0.23 W kg^{-1} at 5 Hz. This value is lower than that of nonbiodegradable actuator of the same type ($50\text{--}160 \text{ W kg}^{-1}$ [43]) and natural muscle ($50\text{--}284 \text{ W kg}^{-1}$ [56]). There are mainly three factors considered for the low specific power. The first is the dielectric strength of the film, which limits the applied voltage for the linear-type actuator. The second is the viscoelasticity of the electrodes, which slows down the movement of the actuator. The third is the mechanical rigidity of the electrodes, mainly defined

as their thickness and modulus. Higher rigidity prevents the actuation, as the electrodes are a passive part. Therefore, the specific power of our actuator will be significantly improved once the components are optimized such that the film has higher dielectric strength and the electrode material has lower viscoelasticity, higher compliance, and thinner form. In addition, decreasing the resistivity of the electrode material allows thinner electrodes because the resistivity depends on the cross section (i.e., thickness and width).

2.3. Circular-Type Biodegradable Electrohydraulic Soft Actuators

Next, we characterized the circular-type actuators in terms of actuated strain and pressure. The tested actuators have different amounts of soybean oil (dielectric liquid): 2 and 4 mL. The applied voltage ranges from 0 to 10 kV with a step size of 1 kV. Figure 6a,b shows the measured strain as a function of the electric field under different loads (8.8, 13.8, and 28.8 g) for actuators with different amounts of soybean oil. As also explained in Experimental Section, a polytetrafluoroethylene (PTFE) sheet (mass 8.8 g) is placed on the actuator so that the laser sensor is able to detect the actuated displacement accurately. Therefore, the loading condition in the experiment starts from 8.8 g. Similar to the case of linear-type actuators, the actuation strain increases with the voltage and reaches 18.6% (2 mL soybean oil) and 9.1% (4 mL soybean oil) at 10 kV under 8.8 g load. The loading results in reduced strain, similar to what is observed for the linear-type actuator. Unlike the linear-type actuators, the circular ones allow

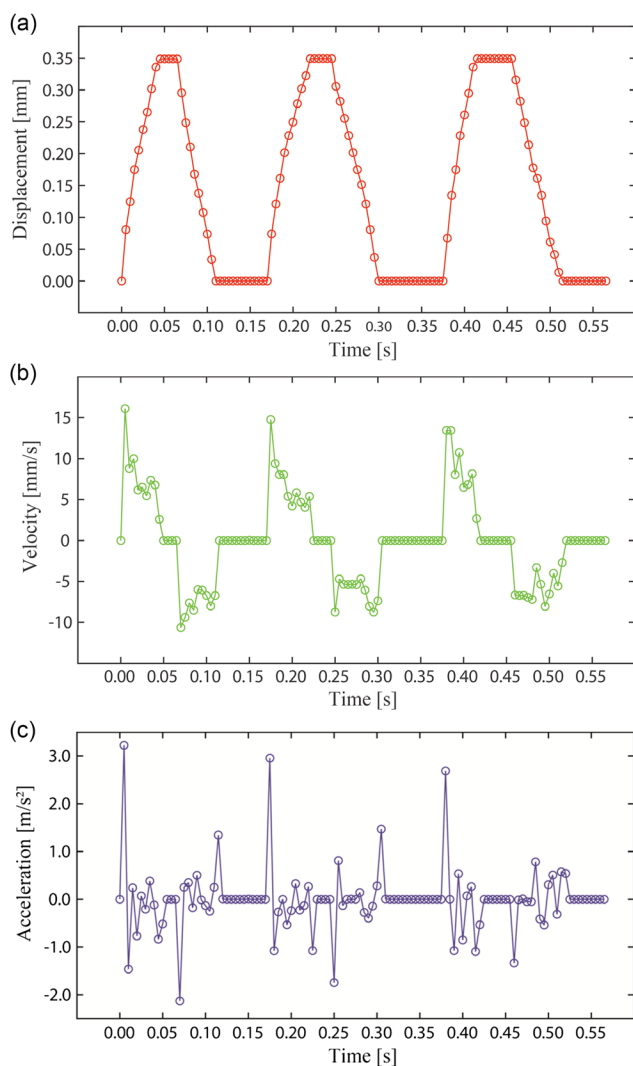


Figure 5. Measured a) displacement, b) velocity, and c) acceleration of linear-type actuator with 5 g load mass (driving frequency, 5 Hz).

the application of voltage up to 10 kV. This is because, during the actuation, the electrodes are always distant, that is, the electric field strength does not exceed the breakdown strength of the pouch layers due to the relatively large amount of soybean oil against the entire volume of the actuator. Estimation of the electrode gap (i.e., the thickness of soybean oil) in the actuator with 18.6% actuation strain, explained in Supporting Information, shows that the oil has $840.8 \mu\text{m}$ thickness, which is expected to be sufficient for withstanding voltages until 10 kV, given that the breakdown strength of soybean oil is up to $58.3 \text{ V } \mu\text{m}^{-1}$ ^[57] and the presence of two layers of dielectric film between the oil and the electrodes. The observed maximum actuation strain 18.6% at 10 kV is within the same range as a nonbiodegradable actuator with identical dimensions (25% at 10 kV^[42]).

In the measured data (Figure 6a,b), a plateau and pull-in transition can be seen, which are described as unique characteristics of actuators of this type.^[42] Pull-in transition is described as a feature when the electrostatic force exceeds the threshold of

the restoring force. In Figure 4b, pull-in transition occurs at 300, 500, and 800 V for under no load, 5 g load, and 20 g load, respectively. In Figure 6a,b, Pull-in transition can be seen at 2, 4, 5, and 10 kV. This behavior has also been reported in the literature.^[42] In the actuator, the electrostatic force between the electrodes scales with the distance between the electrodes. Specifically, this force is known as the Maxwell stress, which is found to be a fundamental principle for soft electrohydraulic actuators in the literature.^[58] Short distance results in larger electrostatic forces, leading to more actuation strain. The amount of dielectric liquid determines the distance between the electrodes and hence the actuation strain, which can be seen in the data shown in Figure 6a,b, where different amounts of liquid (2 and 4 mL) are employed.

Next, we investigated the actuation pressure as a function of the applied voltage. As plotted in Figure 6c, the pressure increases with the voltage and reaches a value of 0.12 kPa at 10 kV, corresponding to a force of 241 mN. The pressure is calculated from the surface area of the load cell fixture in contact with the actuator that has a circular shape with a radius of 25 mm. We further examined the actuation pressure at different actuation strains, from which the force–strain characteristics of the actuators were assessed at 10 kV. As shown in Figure 6d, the pressure reduces as the strain increases, which is also observed in nonbiodegradable actuators of the same type.^[59] For other applied voltages, the actuator is expected to exhibit similar trend; lower voltages result in pressure–strain curves of lower pressure at 0% strain and lower strain at 0 kPa pressure, as demonstrated in nonbiodegradable actuators of the same type.^[59]

Furthermore, to compare the actuation pressure obtained from our actuator (0.12 kPa), the nonbiodegradable circular-type actuator exhibits a value of 25 kPa at 8 kV.^[59] This value is larger than that observed for our actuator, which could be attributed to the difference in the material properties of the dielectric liquids. For instance, a larger dielectric constant leads to a larger electrostatic force and hence a higher pressure. This implies that the output of biodegradable electrohydraulic soft actuators can be increased using dielectric liquids with a high dielectric constant. Nevertheless, the discussed results confirm that the actuators developed in this study function according to the working principle and their actuation performances are comparable to those of the nonbiodegradable ones; this proves the successful implementation of our hypothesis.

3. Conclusion

In this study, we presented biodegradable electrohydraulic soft actuators as electrically driven green robotic elements for environmentally friendly soft robotics. We showed that the electrodes used for the actuators can be tuned to achieve both softness and resistivity suitable for electrically driven soft devices. We also demonstrated the actuators in different forms, with both exhibiting actuation performance comparable to nonbiodegradable counterparts.

In future work, we will focus on the improvement of actuation performance by investigating more suitable biodegradable materials for every part of the actuator. Even though the current device is fully biodegradable, there are any different kinds of biodegradable

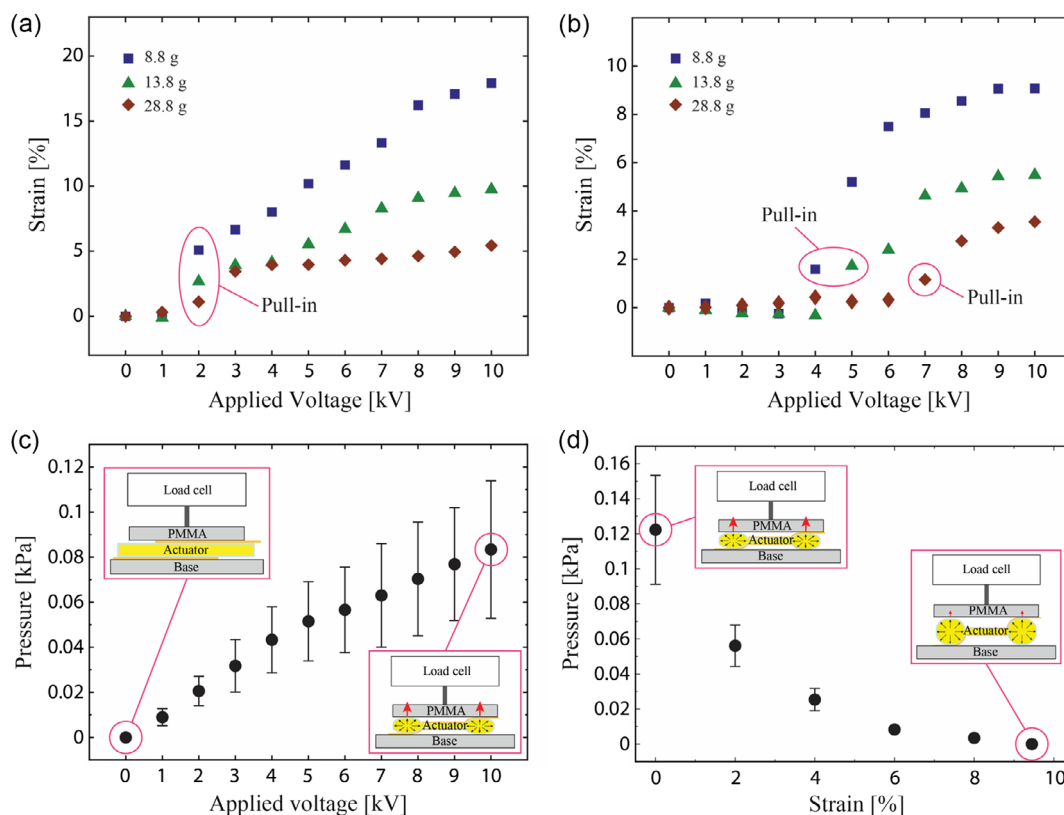


Figure 6. Characterization results of the circular-type actuators. a) Actuation strain as a function of the applied voltage and electric field (amount of dielectric liquid, 2 mL). The voltage to trigger the pull-in transition is 2 kV. b) Actuation strain as a function of the applied voltage and electric field (amount of dielectric liquid 4 mL). Pull-in transition can be seen at 4, 5, and 10 kV for load of 8.8, 13.8, and 28.8 g, respectively. c) Actuation pressure as a function of the applied voltage and electric field. d) Pressure–strain relationship at an applied voltage of 10 kV. The error bars represented in (c) and (d) are the standard deviation calculated from the three samples.

materials that could be implemented for the actuator as an electrode, film, and dielectric fluid. For this purpose, both analytical and computational models are useful. Since the actuator presented in this study consists of dielectric and low-resistivity materials, that is, essential components for electrically driven soft robotic elements, applying the materials to existing working principles may result in biodegradable soft robotic devices of various forms, such as stretchable sensors, electroadhesive pads, and soft pumps. Furthermore, the electrode fabricated in this study is essentially edible, and it can be applied to realize a broad range of devices in edible robotics.

4. Experimental Section

Materials: A dielectric film made of polylactic acid (PLA) and polybutylene adipate-co-terephthalate (PBAT) was purchased from Earth Friendly (“[Biodegradable 100%] Wrap returned to soil”). The thickness of the dielectric film was 10 μm . Gelatin powder (17 009-01) and glycerol (17 029- 00) were purchased from Kanto Chemical. Sodium chloride (NaCl) was purchased from Tomita Pharmaceutical (7647-14-5). Corn starch powder and soybean oil were purchased from a supplier.

Mechanical Characterization of Electrode Material: Gelatin powder was soaked in distilled water and left at room temperature (23 $^{\circ}\text{C}$) for 10 min. The amounts of gelatin powder and distilled water were 30 and 120 g, respectively. Then, glycerol and NaCl were added. The amount

of glycerol was 15 g. The amount of NaCl was 0, 1.25, 2.5, 3.75, and 5 g, which corresponded to the mass fraction relative to the amount of gelatin and glycerol of 0, 2.7, 5.3, 7.7, and 10 wt%, respectively. The mixed materials were dissolved at 80 $^{\circ}\text{C}$ and stirred for 1 h using a hot stirrer (AS ONE, CHPS-170DF). The solution was poured into a mold and cured at room temperature for 1 h. The cured sample was demolded and placed in a humidity chamber (Tolihan, WET-297-AHU) at 23 $^{\circ}\text{C}$ (67% RH) for at least 24 h until testing. The diameter and thickness of the samples were 29 mm and 12.5 mm, respectively. Three samples were used for each material composition (mass fraction of NaCl 0, 2.7, 5.3, 7.7, and 10 wt%). The testing procedure followed was ISO 7743. Each sample was compressed at a speed of 10 mm min^{-1} using a universal testing machine (Shimadzu, AGS-20NX) from which the stress–strain curve was obtained. The testing machine performed four reciprocating motions compressing from 0% to 25% of strain and rebounding from 25% to 0%. The measured force under 20% compressive strain of the fourth round was used to determine the Young’s modulus. It was calculated by dividing the force by the cross-sectional area and strain of the specimen before compression.

Electrical Characterization of Electrode Material: Gelatin powder was soaked in distilled water and left at room temperature for 10 min. The amounts of gelatin powder and distilled water were 30 and 120 g, respectively. Then, glycerol and NaCl were added. The amount of glycerol was 15 g. The amount of NaCl was 0, 0.23, 0.45, 0.69, 0.92, 1.25, 2.5, 3.75, and 5 g, which corresponded to the mass fraction relative to the amount of gelatin and glycerol of 0, 0.5, 1.0, 1.5, 2.0, 2.7, 5.3, 7.7, and 10 wt%, respectively. The mixed materials were dissolved at 80 $^{\circ}\text{C}$ and stirred at 200 rpm for 1 h using a hot stirrer (AS ONE, CHPS-170DF). The solution was then blade casted on a plastic substrate using a film applicator

(Industrial Physics, TQC Sheen) and an applicator coater (Zehntner, ZUA 2000). The blade height of applicator coater was set to 700 μm , and the electrode sheet was cured at room temperature for 24 h at 23 $^{\circ}\text{C}$ (67% RH) to bring it into an equilibrium state. Four samples were prepared for each material composition (mass fractions of NaCl were 0, 0.5, 1.0, 1.5, 2.0, 2.7, 5.3, 7.7, and 10 wt%). The dimensions of the samples were 10 mm in length and 10 mm in width. The surface of the electrode was uniform thanks to the use of film applicator coater, which was used to provide homogeneous film in industry. The thickness of every sample was measured using a laser displacement sensor (OPTEX FA, CDX-L15). Across samples, the thickness was $204 \pm 40 \mu\text{m}$. The electrical resistance of every specimen was measured using a digital multimeter (Keithley, 2100). The value of measured resistance was converted to resistivity by multiplying by the thickness of the electrode.

Fabrication of Biodegradable Electrohydraulic Soft Actuators: The fabrication process is illustrated in Figure S3 and S4, Supporting Information. For the linear-type actuators, two layers of biodegradable dielectric film were bonded by thermobonding in order to encapsulate soybean oil. This was done using a 3D printer (Flashforge 3D technology, Adventurer 3). The print head nozzle of the 3D printer was heated to 180 $^{\circ}\text{C}$, and the platform was kept at 50 $^{\circ}\text{C}$. Two layers of biodegradable dielectric film were overlapped and sandwiched by two layers of polyimide film. By moving the head nozzle to trace over the polyimide film while keeping it in contact with the two layers of biodegradable dielectric film, dielectric films were welded together by heat from the nozzle head. Finally, a pouch of the designed dimensions was fabricated. The width of sealed parts was 5 mm. After a pouch was fabricated, polyimide film was removed. Then, soybean oil was injected into the pouch from the part that was not welded by the 3D printer. The amount of oil used was 1.4 mL. Subsequently, that part was also welded using a soldering iron (HAKKO, FX951), and the pouch was completely sealed. The temperature of the tip of the soldering iron was maintained at 200 $^{\circ}\text{C}$. The gelatin-based electrode was prepared using the same steps as used in the fabrication of samples for the resistivity measurement. The gelatin solution heated at 80 $^{\circ}\text{C}$ for 1 h was blade cast on a plastic substrate using a film applicator (Industrial Physics, TQC Sheen) and an applicator coater (Zehntner, ZUA 2000). The blade height of applicator coater was set to 700 μm , and the electrode sheet was cured at room temperature for 24 h at 23 $^{\circ}\text{C}$ (67% RH) to bring it into an equilibrium state. Then, the cast electrode layer was cut using a plotter cutter (Graphtec, CE6000-40 Plus). The electrode was attached to the pouch made of biodegradable layers by intrinsic adhesion and corn starch powder was coated on it. The fabrication process of the circular-type actuators was the same as that of the linear type, except for the amount of oil used (2 and 4 mL) and the thickness of the electrode layer (blade height of applicator coater: 300 μm).

Characterization of Linear-Type Actuators: The experimental setup is shown in Figure S5, Supporting Information. The characterization was conducted by applying a voltage of up to 1000 V with 100 V incremental to the actuator. The voltage was supplied from a high-voltage DC–DC converter (XP Power, CB101). The actuation strain as a function of the applied voltage was then acquired by measuring the displacement of the actuator tip, which was done using a camera (Nikon, D3500) followed by image processing.

Characterization of Circular-Type Actuators: The characterization process is depicted in Figure S6, Supporting Information. The actuation strain of the actuator was measured using a laser displacement sensor (OPTEX FA, CDX-150). Up to 10 kV of voltage was applied to the actuator with 1 kV incremental. A PTFE sheet (mass 8.8 g) was placed on the actuator so that the laser sensor can detect the actuated displacement accurately. For characterizing the strain–voltage relationship, the actuation force was measured at a certain strain using a linear stage (Thorlabs, PT 1/M), as illustrated in Figure S7, Supporting Information. The force generated by actuation was measured using a load cell (FUTEK, LSB 200). The load cell was placed above the actuator to identify the accurate normal force. The initial load was applied, the mass of which was identical to the PTFE sheet.

Degradation Test of the Actuator: The circular-type actuator was placed on actinomycetes (Okii, Dr. Actinomycete)-mixed soil in an oven (Yamato Scientific, ADP 30 $^{\circ}\text{C}$) at 60 $^{\circ}\text{C}$. The oven had a small hole that allowed air to flow in, which kept the actinomycete active. The soil was collected on the campus of the University of Electro-Communications.

Supporting Information

Supporting Information is available from the Wiley Online Library or from the author.

Acknowledgements

This work was supported by the JSPS KAKENHI Grant-in-Aid for Scientific Research on Innovative Areas “Science of Soft Robot” project (grant number 21H00324).

Conflict of Interest

The authors declare no conflict of interest.

Data Availability Statement

The data that support the findings of this study are available from the corresponding author upon reasonable request.

Keywords

biodegradable, electrohydraulic soft actuators, hydraulically amplified self-healing electrostatic actuators, soft robotics

Received: July 28, 2022

Revised: May 11, 2023

Published online: June 2, 2023

- [1] D. Rus, M. T. Tolley, *Nature* **2015**, 521, 467.
- [2] S. I. Rich, R. J. Wood, C. Majidi, *Nat. Electron.* **2018**, 1, 102.
- [3] M. Cianchetti, C. Laschi, A. Menciassi, P. Dario, *Nat. Rev. Mater.* **2018**, 3, 143.
- [4] M. Ilami, H. Bagheri, R. Ahmed, E. O. Skowronek, H. Marvi, *Adv. Mater.* **2021**, 33, 2003139.
- [5] J. Shintake, V. Cacciolo, D. Floreano, H. Shea, *Adv. Mater.* **2018**, 30, 1707035.
- [6] B. Jumet, M. D. Bell, V. Sanchez, D. J. Preston, *Adv. Intell. Syst.* **2022**, 4, 2100163.
- [7] N. El-Atab, R. B. Mishra, F. Al-Modaf, L. Joharji, A. A. Alsharif, H. Alamoudi, M. Diaz, N. Qaiser, M. M. Hussain, *Adv. Intell. Syst.* **2020**, 2, 2000128.
- [8] P. Polygerinos, N. Correll, S. A. Morin, B. Mosadegh, C. D. Onal, K. Petersen, M. Cianchetti, M. T. Tolley, R. F. Shepherd, *Adv. Eng. Mater.* **2017**, 19, 1700016.
- [9] T. H. Yang, J. Shintake, R. Kanno, C. R. Kao, J. Mizuno, *Adv. Intell. Syst.* **2020**, 2, 2000025.
- [10] J. Shintake, E. Piskarev, S. H. Jeong, D. Floreano, *Adv. Mater. Technol.* **2018**, 3, 1700284.
- [11] J. Shintake, D. Ichige, R. Kanno, T. Nagai, K. Shimizu, *Front. Rob. AI* **2021**, 8, 1.
- [12] F. Schmitt, O. Piccin, L. Barbé, B. Bayle, *Front. Rob. AI* **2018**, 5, 84.
- [13] R. Kanno, T. Nagai, J. Shintake, *Adv. Intell. Syst.* **2021**, 3, 2000173.
- [14] W. B. Li, W. M. Zhang, Q. H. Gao, Q. Guo, S. Wu, H. X. Zou, Z. K. Peng, G. Meng, *Soft Rob.* **2021**, 8, 611.
- [15] Y. Sun, A. Abudula, H. Yang, S.-S. Chiang, Z. Wan, S. Ozel, R. Hall, E. Skorina, M. Luo, C. D. Onal, *Curr. Robot. Reports*, **2021**, 2, 371.
- [16] G. Li, X. Chen, F. Zhou, Y. Liang, Y. Xiao, X. Cao, Z. Zhang, M. Zhang, B. Wu, S. Yin, Y. Xu, H. Fan, Z. Chen, W. Song, W. Yang, B. Pan, J. Hou, W. Zou, S. He, X. Yang, G. Mao, Z. Jia, H. Zhou, T. Li,

- S. Qu, Z. Xu, Z. Huang, Y. Luo, T. Xie, J. Gu, et al., *Nature* **2021**, 591, 66.
- [17] R. K. Katzschmann, J. DelPreto, R. MacCurdy, D. Rus, *Sci. Rob.* **2018**, 3, eaar3449.
- [18] M. T. Tolley, R. F. Shepherd, B. Mosadegh, K. C. Galloway, M. Wehner, M. Karpelson, R. J. Wood, G. M. Whitesides, *Soft Rob.* **2014**, 1, 213.
- [19] O. D. Yirmibeşoğlu, T. Oshiro, G. Olson, C. Palmer, Y. Mengüç, *Front. Rob. AI* **2019**, 6, 1.
- [20] D. Montarnal, M. Capelot, F. Tournilhac, L. Leibler, *Science* **2011**, 334, 965.
- [21] J. M. García, G. O. Jones, K. Virwani, B. D. McCloskey, D. J. Boday, G. M. Huurne, H. W. Horn, D. J. Coady, A. M. Bintaleb, A. M. S. Alabulrahman, F. Alsewilem, H. A. A. Almegren, J. L. Hedrick, *Science* **2014**, 13073, 732.
- [22] D. Neves, P. Sobral, J. L. Ferreira, T. Pereira, *Mar. Pollut. Bull.* **2015**, 101, 119.
- [23] D. J. Shilla, *Tanzania J. Sci.* **2019**, 45, 101.
- [24] J. Shintake, H. Sonar, E. Piskarev, J. Paik, D. Floreano, *IEEE Int. Conf. Intell. Rob. Syst.* **2017**, 2017, 6221.
- [25] M. Baumgartner, F. Hartmann, M. Drack, D. Preninger, D. Wirthl, R. Gerstmayr, L. Lehner, G. Mao, R. Pruckner, S. Demchysyn, L. Reiter, M. Strobel, T. Stockinger, D. Schiller, S. Kimeswenger, F. Greibich, G. Buchberger, E. Bradt, S. Hild, S. Bauer, M. Kaltenbrunner, *Nat. Mater.* **2020**, 19, 1102.
- [26] A. Heiden, D. Preninger, L. Lehner, M. Baumgartner, M. Drack, E. Woritzka, D. Schiller, R. Gerstmayr, F. Hartmann, M. Kaltenbrunner, *Sci. Rob.* **2022**, 7, eabk2119.
- [27] T. Nagai, A. Kurita, J. Shintake, *Front. Rob. AI* **2021**, 8, 383.
- [28] Y. Yamada, *IEEE Rob. Autom. Lett.* **2021**, 6, 3777.
- [29] S. Walker, J. Rueben, T. Van Volkenburg, S. Hemleben, C. Grimm, J. Simonsen, Y. Mengüç, *Int. J. Intell. Rob. Appl.* **2017**, 1, 124.
- [30] A. N. Sardesai, X. M. Segel, M. N. Baumholtz, Y. Chen, R. Sun, B. W. Schork, R. Buonocore, K. O. Wagner, H. M. Golecki, *MRS Adv.* **2018**, 3, 3003.
- [31] M. T. Chorsi, E. J. Curry, H. T. Chorsi, R. Das, J. Baroody, P. K. Purohit, H. Ilies, T. D. Nguyen, *Adv. Mater.* **2018**, 1, 1802084.
- [32] L. D. Chambers, J. Winfield, I. Ieropoulos, J. Rossiter, in *Electroactive Polymer Actuators and Devices 2014* (Ed: Y. Bar-Cohen), International Society for Optics and Photonics, Bellingham, Washington USA **2014**, p. 90560B.
- [33] J. Rossiter, J. Winfield, I. Ieropoulos, in *Electroactive Polymer Actuators and Devices 2016* (Eds: Y. Bar-Cohen, F. Vidal), International Society for Optics and Photonics, Bellingham, Washington USA **2016**, p. 97981S.
- [34] A. Zolfagharian, A. Z. Kouzani, S. Y. Khoo, B. Nasri-Nasrabadi, A. Kaynak, *Sens. Actuators, A* **2017**, 265, 94.
- [35] A. Zolfagharian, A. Kaynak, S. Y. Khoo, A. Z. Kouzani, *3D Print. Addit. Manuf.* **2018**, 5, 138.
- [36] L. Migliorini, T. Santaniello, S. Rondinini, P. Saettone, M. Comes Franchini, C. Lenardi, P. Milani, *Sens. Actuators, B* **2019**, 286, 230.
- [37] L. E. Hanzly, K. A. Kristofferson, N. Chauhan, J. R. Barone, *Green Mater.* **2021**, 9, 157.
- [38] V. Stroganov, M. Al-Hussein, J. U. Sommer, A. Janke, S. Zakharchenko, L. Ionov, *Nano Lett.* **2015**, 15, 1786.
- [39] X. Gao, J. Yang, J. Wu, X. Xin, Z. Li, X. Yuan, X. Shen, S. Dong, *Adv. Mater. Technol.* **2020**, 5, 1900716.
- [40] M. Duduta, D. R. Clarke, R. J. Wood, in *Proc. - IEEE Int. Conf. Robotics and Automation*, IEEE, Piscataway, NJ **2017**, p. 4346.
- [41] P. Rothmund, N. Kellaris, S. K. Mitchell, E. Acome, C. Keplinger, *Adv. Mater.* **2021**, 33, 2003375.
- [42] E. Acome, S. K. Mitchell, T. G. Morrissey, M. B. Emmett, C. Benjamin, M. King, M. Radakovitz, C. Keplinger, *Science* **2018**, 359, 61.
- [43] N. Kellaris, V. G. Venkata, G. M. Smith, S. K. Mitchell, C. Keplinger, *Sci. Rob.* **2018**, 3, eaar3276.
- [44] E. H. Rumley, D. Preninger, A. Shagan Shomron, P. Rothmund, F. Hartmann, M. Baumgartner, N. Kellaris, A. Stojanovic, Z. Yoder, B. Karrer, C. Keplinger, M. Kaltenbrunner, *Sci. Adv.* **2023**, 9, eadf5551.
- [45] R. Kanno, F. Caruso, K. Takai, Y. Piskarev, V. Cacucciolo, J. Shintake, Authorea Prepr. **2022**, <https://doi.org/10.22541/au.166319572.26121427/v1>.
- [46] H. Moustafa, N. El Kissi, A. I. Abou-Kandil, M. S. Abdel-Aziz, A. Dufresne, *ACS Appl. Mater. Interfaces* **2017**, 9, 20132.
- [47] J. Lunt, *Polym. Degrad. Stab.* **1998**, 59, 145.
- [48] F. Miyatake, K. Iwabuchi, *Bioresour. Technol.* **2005**, 96, 1821.
- [49] M. F. Cosate de Andrade, P. M. S. Souza, O. Cavalett, A. R. Morales, *J. Polym. Environ.* **2016**, 24, 372.
- [50] B. G. Hermann, L. Debeer, B. De Wilde, K. Blok, M. K. Patel, *Polym. Degrad. Stab.* **2011**, 96, 1159.
- [51] P. A. Palsikowski, C. N. Kuchnier, I. F. Pinheiro, A. R. Morales, *J. Polym. Environ.* **2018**, 26, 330.
- [52] B. Fasolt, M. Hodgins, G. Rizzello, S. Seelecke, *Sens. Actuators, A* **2017**, 265, 10.
- [53] "Van Der Waals Interactions," [https://chem.libretexts.org/Bookshelves/Physical_and_Theoretical_Chemistry_Textbook_Maps/Supplemental_Modules_\(Physical_and_Theoretical_Chemistry\)/Physical_Properties_of_Matter/Atomic_and_Molecular_Properties/Intermolecular_Forces/Specific_Interactions/Va](https://chem.libretexts.org/Bookshelves/Physical_and_Theoretical_Chemistry_Textbook_Maps/Supplemental_Modules_(Physical_and_Theoretical_Chemistry)/Physical_Properties_of_Matter/Atomic_and_Molecular_Properties/Intermolecular_Forces/Specific_Interactions/Va) (accessed: May 2022).
- [54] D. W. Smith, *J. Chem. Educ.* **1977**, 1, 540.
- [55] P. Veselý, E. Horynová, T. Tichý, O. Šeřil, in *Proc. Int. Student Science Conf. Poster – 22/2018*, Prague, Czech Republic **2018**, p. 1.
- [56] J. D. W. Madden, N. A. Vandesteeg, P. A. Anquetil, P. G. A. Madden, A. Takshi, R. Z. Pytel, S. R. Lafontaine, P. A. Wieringa, I. W. Hunter, *IEEE J. Oceanic Eng.* **2004**, 29, 706.
- [57] A. K. Das, *Electr. Power Syst. Res.* **2023**, 214, 108920.
- [58] S. Kirkman, P. Rothmund, E. Acome, C. Keplinger, *Extreme Mech. Lett.* **2021**, 48, 101408.
- [59] S. K. Mitchell, X. Wang, E. Acome, T. Martin, K. Ly, N. Kellaris, V. G. Venkata, C. Keplinger, *Adv. Sci.* **2019**, 6, 1900178.